Earthq Eng & Eng Vib (2023) 22: 495-511 **DOI**: https://doi.org/10.1007/s11803-023-2180-1

Detailed seismic risk analysis of electrical substation equipment using a reliability based approach

Amir Ghahremani Baghmisheh[1†], Milad Khodaei[2‡], Ali Zare Feiz Abadi[3‡] and Homayoon E. Estekanchi[3§]

1. *Department of Civil Engineering, University of British Columbia, Vancouver V6T 2B8, Canada*
2. *Department of Civil Engineering, University of Tabriz, Tabriz 51666, Iran*
3. *Department of Civil Engineering, Sharif University of Technology, Tehran 11155-9313, Iran*

Abstract: This paper proposes a risk analysis framework for substation structures based on reliability methods. Even though several risk assessment approaches have been developed for buildings, detailed risk analysis procedures for infrastructure components have been lacking in prior studies. The proposed framework is showcased by its application to a system of interconnected structures at a power substation in Tehran. Finite element models of structures are developed and validated in accordance with previous experiments. The uncertainties in the material, mass, and geometric properties of structures are described by random variables that are input to the finite element model. An artificial ground motion model is employed to comprehensively consider uncertainty in ground motion. Monte Carlo sampling is subsequently conducted on the library of probabilistic models. The analysis resulted in the loss distribution in the life cycle of structures. Additionally, the loss associated with six earthquake scenarios having specific magnitudes and return periods is computed. The application provides insight into the most vulnerable equipment in the considered system. Furthermore, introduced risk measures can guide stakeholders to make risk-based decisions to optimize design or prioritize a retrofit of infrastructure components under conditions of uncertainty.

Keywords: seismic risk; reliability analysis; infrastructure components; loss estimation; uncertainty

1 Introduction

This paper puts forward an innovative framework for detailed seismic risk analysis of power substation structures based on reliability methods. The risk analysis in this context involves estimating the exceedance probability (EP) of loss, known as the loss curve. Power substation equipment incurred severe damage from previous earthquakes (Alessandri*et al*., 2015; Gökçe *et al*., 2019). In accordance with earthquake reconnaissance reports (Apostolakis *et al*., 2007; Azevedo *et al*., 2010; Kongar *et al*., 2017; Kwasinski *et al*., 2014), brittle material, slenderness, and huge mass are the main reasons for the notable vulnerability of these structures under ground motion excitations. Damage to equipment may interrupt the functionality of the substation, which in turn leads to disruption of emergency response, business, and recovery procedures. Although several risk assessment methodologies have been developed for various types of buildings — see, for instance, FEMA-P58 (2012) and Ansal *et al*. (2009), D′Ayala and Ansal (2012), Mahsuli and Haukaas (2013b), Narjabadifam *et al*. (2021), Palanci (2019), Papagiannopoulos *et al*. (2012), Shang *et al*. (2020) — risk analysis procedures for substation structures and other infrastructure components have been inadequately investigated in the literature (Zheng and Li, 2022). Thus, developing a comprehensive risk analysis procedure for infrastructure components, especially electrical equipment, is of great importance.

Several risk assessment methodologies have been developed at the regional and structural levels in recent years. The Applied Technology Council proposed the ATC-13 approach (1985), the first comprehensive procedure for seismic damage evaluation at the regional level. This approach used the subjective opinions of experts to estimate damage and loss at various values of modified Mercalii intensity. Two decades later, the Federal Emergency Management Agency (FEMA) of the U.S. proposed the HAZUS methodology (FEMA, 2003), which employed the capacity spectrum method. Unlike the ATC approach, this methodology accounts for the mechanical properties of structures in damage evaluation. Cornell and Krawinkler (2000) suggested a risk analysis procedure based on conditional probability

Correspondence to: Amir Ghahremani Baghmisheh, Department of Civil Engineering, University of British Columbia, 2721 Fairview Crescent, Vancouver V6T 2B8, Canada
Tel: +1-2368692459
E-mail: amirghb@mail.ubc.ca
†PhD Candidate; ‡MSc Graduate; §Professor
Received March 10, 2022; **Accepted** October 10, 2022

models and the total probability theorem, presented in greater detail by Moehle and Deierlein (2004). This procedure utilizes probabilistic models representing the distribution of hazard, response given hazard, damage given response, and loss given damage. These models were combined using the total probability theorem, forming a triple integral, entitled PEER triple integral. Yang *et al*. (2009) solved this integral by using a sampling-based procedure to obtain loss distribution. This procedure is then incorporated in the FEMA-P58 (2012) as a detailed risk analysis methodology for buildings. Mahsuli and Haukaas (2013b) proposed an alternative procedure wherein a chain of interacting probabilistic models are subjected to a reliability analysis to estimate the exceedance probability of loss, i.e., the loss curve. They demonstrated its application in the Vancouver, Canada, metropolitan region. In the regional risk analysis, simple models were utilized to estimate the EP of loss. For instance, the intensity of an earthquake is computed by using ground motion prediction models; or, simple regression models can predict the overall response of structures. Thus, this procedure provides a rough estimate of loss. The present study extends reliability-based risk analysis to a more detailed level, by which more refined models are employed to simulate ground motion and the response of infrastructure components.

The combinations of reliability and finite element methods have been extensively investigated in the literature (Altieri *et al*., 2018; Der Kiureghian and Zhang, 1999; Jahangiri and Shakib, 2020; He and Li, 2004; Mohsenian *et al*., 2021; Shang *et al*., 2020; Sudret and Der Kiureghian, 2002), and seismic reliability-based design approaches are proposed for various structural systems (Castaldo *et al*., 2016, 2017, 2018). Reliability-based performance evaluation of structures in the literature involves a limit state function that defines the failure state of the component. The expected cost is obtained by summing construction costs with the multiplication of the failure probability by the cost of failure. In contrast, this study considers the total cost as a random variable whose probability distribution depends on numerous probabilistic models and random variables predicting the hazard, response, damage, and loss.

Seismic damage assessment of power infrastructure components has been the subject of numerous studies, (Baghmisheh and Estekanchi, 2020, 2021; Bai *et al*., 2017; Mohammadi *et al*., 2012; Mohammadi and Tehrani, 2014; Wen *et al*., 2019; Yang *et al*., 2021) among others. Zareei *et al*. (2017) investigated the vulnerability of high-voltage circuit breakers with the use of bivariate fragility models. Paolacci *et al*. (2014) developed an analytical fragility curve for a 380 kV disconnect switch and carried out a sensitivity analysis to determine the effects of model parameters. Baghmisheh and Estekanchi (2019) developed analytical fragility models for four interconnected components of substations. They examined the effects of conductors between equipment on the amplification of responses and the fragility of that equipment. Zheng *et al*. (2017) investigated the progressive collapse of steel power transmission towers under ground motion. Moreover, probability of collapse was evaluated based on fragility curves. Yang *et al*. (2017) addressed the failure probability of towerline systems using incremental dynamic analysis. Baghmisheh and Mahsuli (2021) examined seismic damage patterns and the collapse probability of concrete power poles by means of the dynamic analysis of detailed finite element models. Even though estimating seismic damage and the subsequent failure probability of power components has been broadly discussed, a comprehensive approach for evaluating seismic loss of equipment is missing from the literature.

This study aims to develop a detailed reliability-based risk analysis framework for substation equipment that explicitly accounts for all substantial uncertainties involved in loss estimation. Even though few studies have investigated detailed seismic risk analysis of buildings by using reliability methods (Aghababaei and Mahsuli, 2018), the application of reliability methods to detailed seismic risk analysis of infrastructure components is presented in this study for the first time. Although some classic reliability analyses have been conducted to compute the failure probability of substation structures (Bagen *et al*., 2019; Kulhawy *et al*., 2007; Li *et al*., 2019), none of them extended the application of reliability methods to explicitly calculate the probability distribution of loss. The proposed procedure utilizes random variables and probabilistic models to account for uncertainty in hazard, response, and loss. In contrast to the approach based on the total probability theorem, probabilistic models are not conditional herein. That is, they receive realizations of random variables as input and produce a measurable physical parameter rather than a probability. This enables the employment of finite element models in a probabilistic framework. To conduct risk analysis, the limit state function is defined on the monetary loss of equipment. Then, a chain of interacting probabilistic models is constructed and subjected to Monte Carlo sampling to estimate the EP of loss. This framework is showcased by its application to a system of interconnected structures at a power substation in Tehran. Furthermore, this study discusses various risk measures derived from the loss curve. Each of these measures can be used to optimize the design of infrastructure components in accordance with the attitude of the designer toward risk, i.e., risk-neutral or risk-averse.

The paper begins by describing the risk analysis approach. Then, it proceeds to introduce probabilistic models used in detailed risk analysis. Application of the proposed procedure in the seismic risk analysis of a system of substation equipment under various earthquake scenarios is subsequently discussed. The paper concludes by introducing four risk measures to summarize risk analysis results that yield insight into differences among various measures.

2 Risk analysis approach

The two main components of each reliability method are random variables and limit state functions. Random variables represent prevailing uncertainty in a system. Limit state functions define the failure state of the system. In the classic application of reliability methods, the failure probability of the system is computed by defining the limit state function on demand and capacity. To extend the application of reliability methods to risk assessment, the limit state function is defined regarding the consequences of an earthquake, such as direct economic loss based on Haukaas′s study (Haukaas, 2008). The objective of adopting the limit states is to calculate the exceedance probability of losses from a specific threshold. For instance, the limit state function for computing the EP of the direct loss of two structures that was considered in the application of this study, i.e., surge arrester (SA) and current transformer (CT), from a specific threshold, l_0, is as follows:

$$g(\boldsymbol{x}) = l_0 - (l_{\mathrm{SA}}(\boldsymbol{x}) + l_{\mathrm{CT}}(\boldsymbol{x})) \tag{1}$$

where l_{SA} and l_{CT} , respectively, denote the direct loss of SA and CT, and $\boldsymbol{x}$ is a vector containing random variables representing uncertainties. The reliability method computes the probability that the limit state function is equal to or less than zero by numerically calculating the following multiple integral:

$$p = \int \cdots \int_{g(\boldsymbol{x}) \le \mathbf{0}} f_x(\boldsymbol{x}) \mathrm{d}\boldsymbol{x} \tag{2}$$

in which $f_x(\boldsymbol{x})$ is the joint probability distribution function of random variables. The number of integral operators is the same as the number of random variables in the $\boldsymbol{x}$ vector. The integration is performed in a region where $g(\boldsymbol{x}) \le 0$. The calculation of the integral leads to a single point on the distribution of economic loss, i.e., the loss curve. Repeating this procedure for various thresholds, l_0, in the limit state function yields the loss curve. Among various reliability methods developed to solve the multifold integral in Eq. (2), Monte Carlo sampling is applied in this study. This method uses the below expression to calculate the multiple integral:

$$p = \int_{-\infty}^{+\infty} \cdots \int_{-\infty}^{+\infty} \psi(g(\boldsymbol{x})) \cdot f_x(\boldsymbol{x}) \mathrm{d}\boldsymbol{x} \tag{3}$$

where ψ is a binary function taking the value of 1 when the limit state function is less than zero, and zero when the limit state function is greater than zero. In each sample of Monte Carlo sampling, a realization of random variables is produced according to their joint probability distribution and the ψ function is computed. Performing sampling using K samples leads to the specification of desired probability, as follows:

$$p = \frac{1}{K} \sum_{k=1}^{K} \psi_k \tag{4}$$

where ψ_k denotes the value of the ψ function for the sample of k, and K is the total number of samples.

The scenario sampling method proposed by Mahsuli and Haukaas (2013b) is adopted in this study for risk analysis of substation equipment. This method is a derivation of Monte Carlo sampling, making multi-hazard risk analysis possible. It also enables taking into account time-dependent phenomena such as degradation in risk analysis or discounting economic losses to the present value. In this approach, scenarios with an arbitrary length of time, for instance, 50 years, are assumed, and the considered system is subjected to hazards that occurred during the scenario. For instance, the limit state function accumulated loss over a 50-year period and is computed at the end of each scenario. Simulating too many scenarios yields the desired probability of exceedance.

Conducting seismic risk analysis using scenario sampling requires a chain of probabilistic models from the earthquake occurrence model to the loss model. Figure 2 illustrates the probabilistic models employed in this study, and Table 1 lists the characteristics of the input and output parameters of each model. Each box in Figure 2 represents a probabilistic model. The symbols entering the model from the top of the box are random variables or constant values, and those entering the model from the left side are the responses of upstream models. A detailed explanation of each model will be presented in the following section. These models are utilized here to explain the procedure of the analysis. By starting from the left side, the occurrence model of each seismic source specifies the occurrence of earthquakes, together with the time of occurrence during the span of the scenario. The magnitude and location models specify the magnitude and rupture location of the earthquake. Next, these values are entered into the artificial record generation model to produce an artificial ground motion in accordance with the magnitude and distance of the epicenter from the site. Then, the numerical model of the system is subjected to input excitation, and the maximum of responses is estimated. The structural responses are treated as input to the loss model, which computes the ensuing loss damage. That loss is subsequently discounted to the present value by using a discounting model. The result of this procedure is the discounted economic loss for one earthquake occurrence in the span of a scenario. The procedure is repeated for other earthquake events in the scenario, and the losses are summed for all events. The accumulated loss value enters the limit state function in Eq. (1). Finally, simulating enough scenarios results in the EP of the sum of losses from a threshold, i.e., l_0. An overview of the explained methodology is demonstrated in the flowchart

shown in Fig. 1. In this figure, all random variables are summed in vector $\boldsymbol{x}$. The response of each model denoted by $\boldsymbol{r}_n$. The accuracy of this approach in calculating the desired probability depends on the number of simulated scenarios. A criterion for evaluating this accuracy is the coefficient of variation of the computed probability per (Mahsuli and Haukaas, 2013b):

$$CoV(p)=\sqrt{\frac{1}{K-1}\cdot\frac{1-p}{p}} \tag{5}$$

Note that the scenario sampling method requires high computational effort. On the other hand, the possibility of considering time-dependent phenomena such as the accumulation of loss during the event time and discounting costs to the present value are advantages of this method. Furthermore, the whole loss curve can be determined by a single scenario sampling analysis, while other reliability methods, such as the first-order reliability method (FORM), necessitate individual analysis for calculating each point on the loss curve.

As mentioned, the scenario sampling procedure

Table 1 Overview of parameters of probabilistic models shown in Fig. 2

Symbol	Description	Parameter type	Characteristics
b_i'	Distribution parameter for source i magnitude	Random variable	LN(μ,σ)
C_{cj}	Replacement cost of equipment j	Random variable	LN(μ,σ)
d	Artificial ground motion duration	Constant	25 s
$\boldsymbol{D}$	Vector of the outer dimension of insulators	Random variable	U(a, b)
D_{p}	Density of porcelain material	Random variable	LN(μ, σ)
d_i	Source i depth	Model response	
F	Fault type	Constant	
F_{y}	Yield strength of support structure elements	Random variable	LN(μ, σ)
L_{ai}	Source i rupture location latitude	Model response	
$\boldsymbol{L}_{\mathrm{s}}$	Vector of substation coordinates	Location	35°18’50.72”N, 51°38’8.61”E
l_j	Equipment j repair cost	Model response	
l_{T}	Total direct economic loss	Model response	
L_{oi}	Source i rupture location longitude	Model response	
$\boldsymbol{M}$	Vector of concentrated mass of equipment	Random variable	LN(μ, σ)
m_i	Source i earthquake magnitude	Model response	
$M_i^{\max}$	Source i maximum magnitude	Random variable	LN(μ, σ)
$M_i^{\min}$	Source i minimum magnitude	constant	4.8
PGA	Peak ground acceleration	Model response	
r	Effective interest rate		N(0.03, 0.003)
t	Time parameter	Time	
T_{s}	Time span	Constant	50 years
$\ddot{\boldsymbol{u}}_{\mathrm{g}}$	Vector of acceleration time history	Model response	
V_{s}	Shear wave velocity at the substation site	Random variable	U(760, 1500)
$\sigma_{\max}$	Maximum stress at the bottom of the insulator	Model response	
σ_{u}	Ultimate strength of porcelain	Random variable	LN(μ, σ)
Δt	Acceleration history time step	Constant	0.02 s
ε_{cj}	Equipment j repair cost error	Random variable	N(1, 0.1)
$\boldsymbol{\varepsilon}_{\mathrm{GM}}$	Vector of six regression errors of ground motion model	Random variable	
ε_{ai}	Source i latitude geometric uncertainty	Random variable	L(0, 0.02)
ε_{oi}	Source i longitude geometric uncertainty	Random variable	L(0, 0.02)
θ_{mi}	Source i magnitude uncertainty	Random variable	N(0, 1)
θ_{oi}	Source i location uncertainty	Random variable	U(0, 1)
λ_i	Earthquake occurrence rate of source i	Random variable	LN(μ, σ)
$\boldsymbol{\omega}$	White-noise vector	Random variable	N(0, 1) for each element of vector

yields accumulated loss, to which each seismic source contributes according to its occurrence rate. The procedure can also be used to calculate the loss of equipment associated with the occurrence of an earthquake with a specific magnitude or return period (RP). That is, the occurrence of an earthquake event is independent of its source's rate; hence, an earthquake with a specific scenario, e.g., M=7, occurs in each sample. In particular, the occurrence model is omitted from the chain of models shown in Fig. 2, and the magnitude

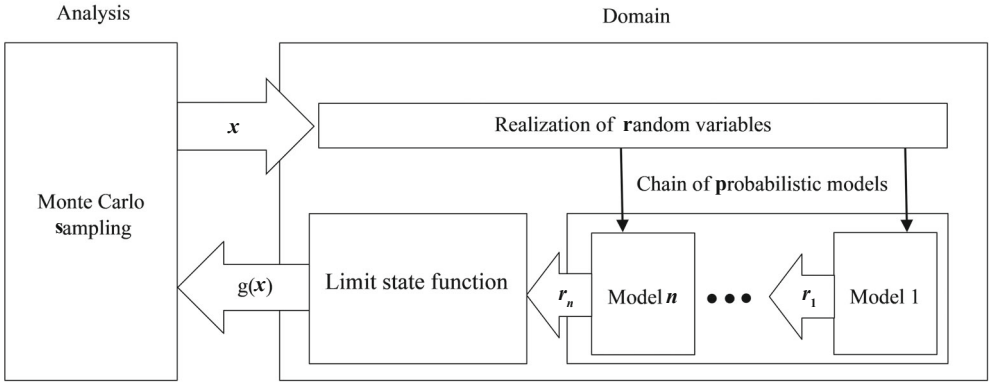

Fig. 1 Overview of the analysis methodology

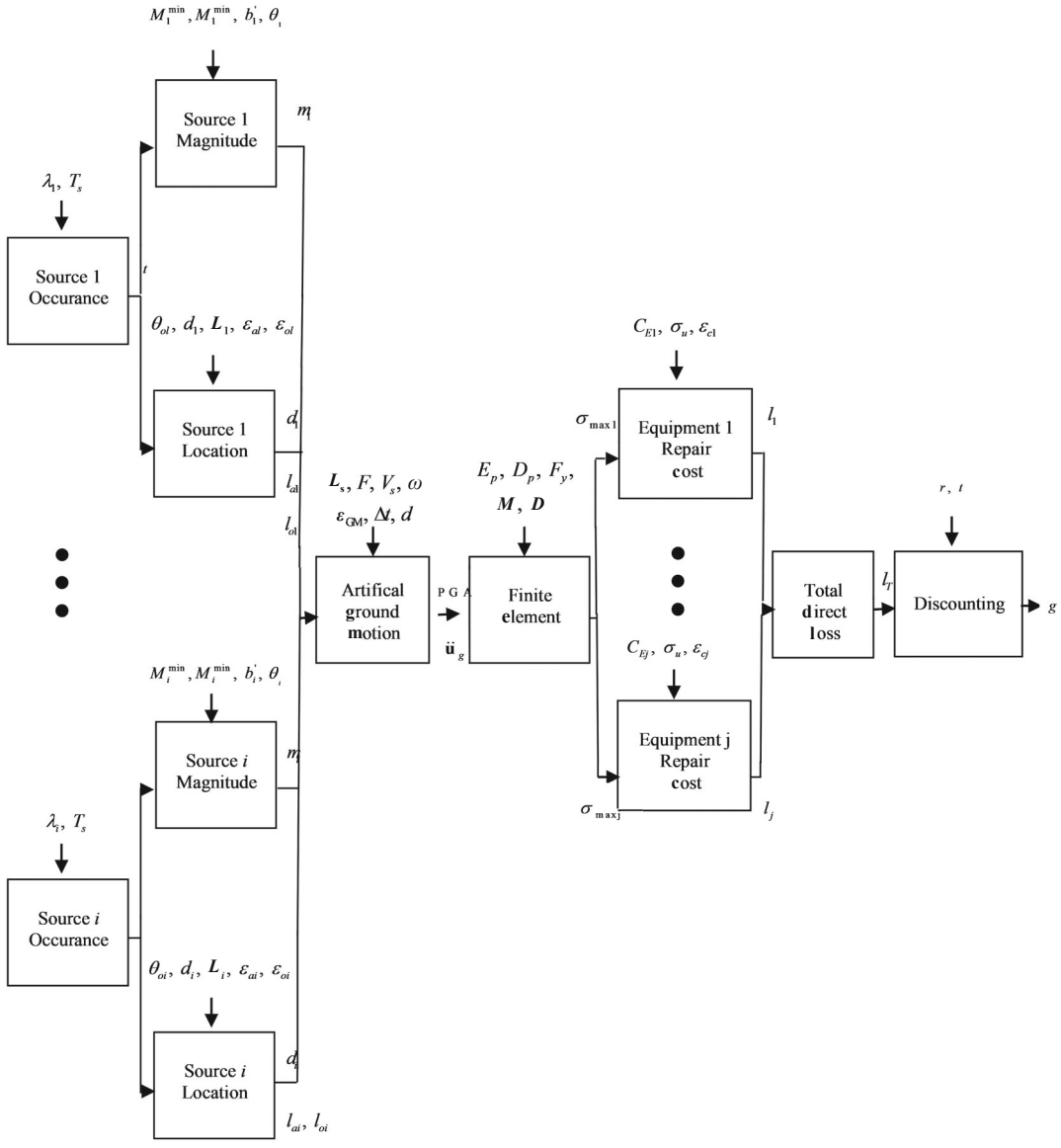

Fig. 2 The chain of the probabilistic models employed in the seismic risk analysis of substation equipment

model is substituted by a constant value, for instance, M=7. This procedure also makes it possible to consider earthquakes with a specific return period, e.g., 2,475 years. For this purpose, the peak ground acceleration (PGA) of the intensity model for each sample is scaled to the PGA corresponding to the specific return period in the hazard curve of the site. The application of this procedure for various earthquake scenarios is demonstrated in Section 4.1.

3 Probabilistic models

As the preceding section explains, seismic risk analysis of substation equipment using the proposed method requires a library of probabilistic models. Those models should follow a set of rules to be usable in the reliability-based approach (Mahsuli and Haukaas, 2013a): (1) random variables, as input to the model, represent uncertainty; (2) for each individual realization of random variables, the model produces a unique, measurable physical output. The general form of probabilistic models is explained in the following sections. Additionally, the individual inputs that each model requires for the seismic risk analysis of substation equipment are provided. Note that the occurrence, magnitude, location, and intensity models are adopted from the literature and adjusted to be appropriate for application in this study.

3.1 Occurrence model

The well-known point process of Poisson is adopted to model the occurrence of the earthquake in time. This model takes the rate of the seismic source as input and produces the occurrence time of an earthquake within the considered time period, for instance, 50 years. The characteristics of the two seismic sources surrounding the considered substation are listed in Table 2 per Mahsuli *et al*. (2018). The parameters of this table are explained in subsequent sections.

3.2 Location model

The location model specifies the rupture location along the length of the seismic source. In some studies, such as Kiureghian and Ang (1977), the probability distribution function is proposed for the distance between the site and the rupture location. Even though these functions can be used in reliability-based risk analysis as random variables, the close distance between the equipment located in a substation and the correlation of intensities each piece of equipment undergoes makes the employment of these functions difficult. Hence, the location model developed by Mahsuli and Haukaas (2013a) is utilized here. This model takes random variables introduced in Table 1 as input and generates the rupture location as output. In this model, linear seismic sources are modeled by specifying the longitude and latitude of multiple segments of the source. The uncertainty in the rupture location is represented by four random variables. The first two quantify uncertainty in the longitude and latitude of the source′s corners. Each realization of these random variables leads to the coordinate of the segments′ corners. The third random variable, distributed uniformly, quantifies the uncertainty of the rupture location along the length of the fault. Finally, the fourth random variable models the depth of the rupture. The two first random variables were absent in the primary model, as proposed by Mojtaba Mahsuli *et al*. (2018). The rupture is always located on the length of the fault in the primary model, while the introduction of new random variables yields to ruptures around the fault, which is more realistic. By specifying the rupture location, the distance between each arbitrary site to the rupture location can be easily evaluated. Figure 3 indicates the geometry of the two line sources utilized in the location model of the procedure′s application.

3.3 Magnitude model

The magnitude model generates the moment magnitude, m, for each seismic source. Most of the existing studies in the literature (for instance, McGuire (2004)) propose the probability distribution of magnitude.

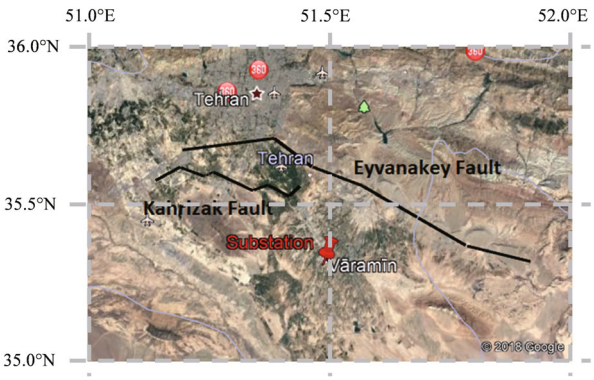

Fig. 3 Geometry of the seismic sources and location of the substation. Map data from Google

Table 2 Characteristics of the two seismicity sources surrounding the substation

Source name	b'		M^{max}		λ (per year)	
	Mean	SD	Mean	SD	Mean	SD
Eyvanakey	1.64	0.07	7.98	0.23	0.034	0.008
Kahrizak	1.64	0.07	7.98	0.23	0.011	0.003

The one adopted here is based on the work of Mahsuli *et al*. (2018), in which one of the magnitude models in the literature was modified using the probability preserving equation, so that it would be appropriate for reliability analysis. The relationship of this model reads:

$$m = -\frac{1}{b'}\ln\cdot\left[1-\Phi(\theta_m)\cdot(1-\exp(-b'(M^{\max}-M^{\min})))\right]+M^{\min} \tag{6}$$

In this equation, b' is a parameter that depends on the relative occurrence rate of different magnitudes. $M^{\min}$ and $M^{\max}$ are respectively the lower and upper bound of the magnitude that the seismic source can generate. θ_m is a variable with standard normal distribution, which transfers the probability distribution of the magnitude to the above-mentioned equation. Since b' and $M^{\max}$ incorporate uncertainties, random variables are adopted to represent them. Table 2 lists the mean and standard deviation of these parameters for each seismic source. Mahsuli *et al*. (2018) found that neglecting the uncertainty of these parameters and using average values results in a considerable error at the tail of magnitude distribution. Thus, the uncertainty of these parameters is taken into account. Once realizations of each random variable, i.e., b', $M^{\max}$, and θ_m, are generated for each sample, Eq. (6) estimates the magnitude.

3.4 Ground motion intensity model

Numerous attenuation relationships exist in the literature that estimate the intensity at the site location using magnitude and the distance between the site and the rupture location. To fulfill the objective of this study, namely, a detailed seismic risk analysis of substation equipment, the intensity at the substation location is not sufficient. There is a need to establish the time history record of ground motions. Therefore, the appropriate intensity model should be able to produce time history records. Although natural ground motions can be employed in the proposed approach, finding a large set of natural ground motions consistent with the properties of the site is almost impossible. Furthermore, even using an extensive suite of natural ground motions cannot incorporate the complete uncertainty of ground excitation (Aghababaei and Mahsuli, 2018). Hence, a model producing the artificial record is employed herein. This model produces frequent and nonfrequent ground motions as defined in Paolo Castaldo and Amendola (2021), Kitayama and Constantinou (2019), according to the inputs for magnitude and distance from upstream models. The model was first introduced by Rezaeian and Der Kiureghian (2012) and implemented in the Rt (Mahsuli and Haukaas, 2012), a software designed for reliability analysis by Aghababaei and Mahsuli (2018). The non-stationarities involved in the temporal and spectral characteristics of ground motions are considered in this model.

An acceleration process, $x(t)$, is specified in the core of the adopted model as the response of a linear filter to a white noise process, as expressed in the following:

$$x(t) = q(t,\boldsymbol{\alpha}_{\mathrm{g}})\cdot\frac{1}{\sigma_h(t)}\int_{-\infty}^{t} h\left[t-\tau,\lambda(\tau)\right]\boldsymbol{\omega}(\tau)\mathrm{d}\tau \tag{7}$$

in which $q(t, \boldsymbol{\alpha}_{\mathrm{g}})$ denotes the time-modulating function wherein the duration, shape, and intensity of the motion are controlled by the $\boldsymbol{\alpha}_{\mathrm{g}}$ factor; $\sigma_h^2(t)$ denotes the integral processes′ variance; $h\,[t\text{-}\tau, \lambda(\tau)]$ denotes filter′s impulse response function in which $\lambda(\tau)$ collects time-varying parameters; and $\boldsymbol{\omega}$ denotes the white noise process. The temporal characteristics of the process are described by $q(t, \boldsymbol{\alpha}_{\mathrm{g}})$, and the spectral characteristics of the process are described by $h\,[t\text{-}\tau, \lambda(\tau)]$. The components of two vectors, i.e., $\boldsymbol{\alpha}_{\mathrm{g}}$ and $\lambda(\tau)$, are dependent upon six characteristics of ground motions The $\boldsymbol{\alpha}_{\mathrm{g}}$ vector consists of three components that depend on the time at the middle of strong motion, t_{mid}, the effective duration of excitation, $D_{5\text{-}95}$, and the Arias intensity, I_a, The $\lambda(\tau)$ vector consists of two functions that are dependent on the damping of the filter, ξ_{f}, the rate of variation of filter frequency in time, ω', and the frequency of the filter at the middle of strong motion, ω_{mid}. Finally, a high pass filter passes $x(t)$ to ensure the residual displacement and velocity of the ground motion are zero.

Regression models developed by Rezaeian and Der Kiureghian (2012) produce the aforementioned parameters by considering the moment magnitude, the distance between the site and rupture location, the speed of the shear wave at a depth of 30 m, and the mechanism of rupture as input. In the present study, the two first parameters are produced by the upstream magnitude and location models; the last two parameters are specified in accordance with the characteristics of the site and faults. It should be noted that the regression models were calibrated in Rezaeian and Der Kiureghian (2012) according to a large set of previous earthquakes data. The 6×6 covariance matrix of models′ errors, denoted by $\boldsymbol{\varepsilon}_{\mathrm{GM}}$ in Table 1, were produced through calibration. The errors of regression models are presented herein by random variables. These errors explicitly account for the epistemic uncertainty involved in ground motion. On the other hand, the white noise utilized in the model takes into account aleatory uncertainty in ground motion. Further details on the artificial record model can be found in Rezaeian and Der Kiureghian (2012).

In the application of the proposed method, the artificial record model is utilized to generate the input excitation for each seismic source. The reverse mechanism is assumed for seismic sources. According to the soil type of the site, type B per ASCE7/SEI 16 (2017), the speed of the shear wave, is modeled by using a uniformly distributed random variable with lower and upper bounds of 760 and 1500 m/s^2.

3.5 Structural response model

The structural response model is a finite element

model that receives the required inputs from upstream models and produces the structural response utilized in the ensuing damage or loss models. Owing to the fact that the reliability analysis generates measurable physical parameters as input for the structural response model, any finite element code or software is applicable here. As a case in point, the finite element model of a system of interconnected electrical equipment is developed in OpenSees software (McKenna *et al*., 2000) as the structural response model. The system consists of a high-voltage surge arrester and a current transformer, two components that are common in electrical substations. These pieces of equipment are connected to each other through a rigid bus bar. Figure 4 shows the configuration of the surge arrester-current transformer (SACT) system. The central part of the equipment consists of slender porcelain columns, which increase the seismic vulnerability of the equipment. Steel or cast iron flanges connect porcelain columns. The previous experimental studies (Alessandri *et al*., 2015; Takhirov *et al*., 2004) on the porcelain column-flange systems demonstrate a linear elastic behavior for this system. The bus bars connecting the two pieces of equipment are composed of a flexible connector, known as a bus slider (BS), which introduces nonlinearity to the SACT system. Due to the linear behavior of stand-alone equipment, modal analysis is used to verify the numerical model of the equipment. On the other hand, cyclic tests on the BS are employed to verify the response of this component.

Now attention turns to developing finite element models. The complex geometry of porcelain columns and flanges makes difficult the calculation of flexural stiffness of these components. Thus, regression models proposed by Li *et al*. (2017), which are calibrated through the use of 12 experimental tests, are employed. These models provide the geometry details of porcelain column and flange connectors as input and calculate the flexural stiffness of columns and joints. By using calculated stiffness, columns and joints are modeled by elastic beam-column elements and zero length springs, respectively. The steel supporting structure of equipment is modeled by using nonlinear DispBeamColumn elements. The nonstructural components at the top of equipment, i.e., the oil reservoir and ring, are treated as concentrated mass. Key structural parameters of equipment and their supporting structures are respectively listed in Table 3 and Table 4.

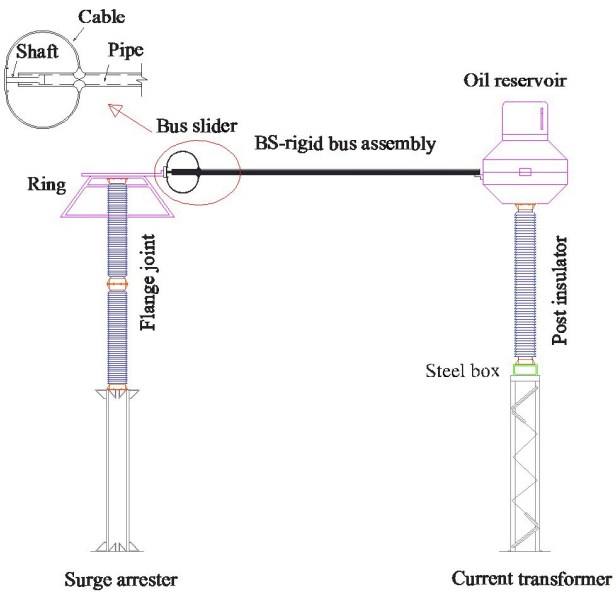

Fig. 4 Schematic view of the surge arrester-current transformer system

Modal analysis is carried out on the individual equipment to verify the stand-alone model for the equipment. The first natural frequency of the surge arrester, tested by Li *et al*. (2017), is calculated as 2.2 Hz through the simulation carried out in this study. This is in good agreement with the first natural frequency of 2.0 Hz obtained in the experiment. The first natural frequency of the current transformer without the supporting structure is estimated as 3.79 Hz, which is consistent with the frequency of 3.80 Hz provided by the manufacturer.

The bus bar and bus slider of the conductor are modeled by the elastic beamcolumn elements and a nonlinear axial spring, respectively. To characterize nonlinear behavior of BS, the cyclic test conducted on the BS by Filiatrault (2000) is utilized. The parameters of steel01 material are adjusted to reproduce the test results. Figure 5 compares the hysteresis curves of the simulation with those obtained in the test. The comparison reveals that the simulation captures the hysteretic cycles observed in the experiment with reasonable accuracy. Note that geometric nonlinearity and material nonlinearity of the connector and the supporting structure are the sources of nonlinearity in the considered system. However, dynamic analyses show that supporting structures do not experience nonlinear behavior before failure of porcelain. Figure 6 depicts a schematic view of the developed numerical model for the interconnected system. Note that since the connection between the equipment is explicitly modeled in the numerical model, the beneficial or detrimental effects on seismic response are automatically considered in the results. In most cases, since the conductor has not reached its maximum deformation capacity, its effect on the seismic response was beneficial. This is mainly due to energy dissipated in the conductor.

According to the existing literature (such as Bayari *et al*. (2022) or Gino *et al*. (2021)), the response of nonlinear numerical model is always affected by epistemic uncertainty. In order to account for the modeling uncertainty, parameters associated with the geometry, material, and mass of the model are represented by random variables in this study. The distribution of random variables is specified using mean values of the deterministic model and assuming a coefficient of variation. The lognormal distribution models′ uncertainties are associated with material and mass properties, while the uniform distribution models

are those associated with geometric properties. The second-moment parameters of each random variable are respectively summarized in Table 5 and Table 6 for lognormal and uniform distribution. Note that the distribution of random variables should be determined in accordance with tests conducted on the material in a real-world application of the procedure. Since this study aims to demonstrate the application of the proposed procedure, assumptions for the distribution of random variables are justified.

In order to incorporate the finite element model in the reliability analysis, the connection is made between the finite element software, OpenSees, and the reliability analysis software, Rt. Realizations of random variables at each step of the reliability analysis yield a new numerical model for the system. Thereafter, the numerical model is subjected to artificial ground motion. Thus, time history analysis is conducted at each step of reliability analysis to produce structural responses. According to IEEE 693 (2005) recommendations, a 2% damping ratio associated with the first and second modes is considered in analyses. The mass and stiffness proportional factors of Rayleigh′s method are considered to be 0.467 and 0.00085, respectively. As convergence criteria, the norm displacement increment with a maximum of 100 iterations and 1.0×10^{-8} tolerance is employed. The distribution of key response parameters is presented in Section 4. These responses are treated as input for the repair model described in the following section.

3.6 Repair cost model

This section describes the repair cost model that calculates the monetary loss of induced damage. According to reconnaissance reports of previous earthquakes (Jaigirdar, 2005; Khalvati and Hosseini, 2009; Takada *et al.*, 2004), most damage is incurred in the porcelain part of the substation equipment. Formation of cracks, leaking of oil, and crushing of porcelain are among the damage observed in previous earthquakes. Similar to previous studies (Baghmisheh and Estekanchi, 2019; Mohammadpour, 2017; Zareei *et al.*, 2017), two damage states, “moderate” and “extensive”, are considered here. The moderate damage state is associated with forming fine cracks on the outer surface of the porcelain, and the extensive damage state is related to the formation of large cracks, which leads

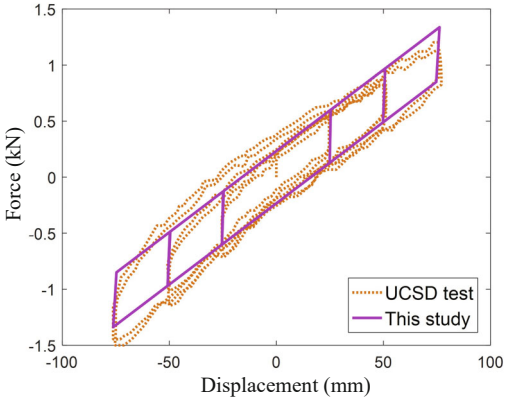

Fig. 5 Comparison between hysteresis cycles observed in the test by Filiatrault (2000) and those obtained in the simulation

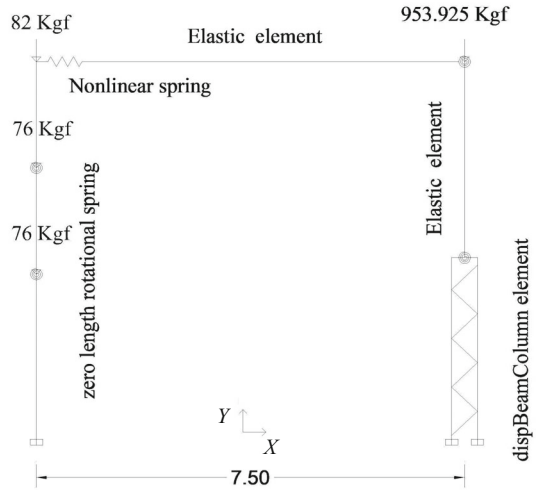

Fig. 6 Schematic view of the numerical model

Table 3 Key parameters of equipment

Equipment	Position of porcelain unit	Flange joint stiffness (N·m/rad)	Height (m)	Outer diameter (m)	Inner diameter (m)	Weight (N)
Surge arrester	Top	13.55×10^{6}	1.88	0.37	0.353	2530.98
	Bottom	13.55×10^{6}	1.88	0.37	0.353	2530.98
Current transformer	Top[1]	$24.19\ (11.04)\times 10^{6}$	3.46	0.48	0.442	8103.75

[1] Flange stiffness at the top of units (flange stiffness at the bottom of units).

Table 4 Key parameters of supporting structures

Equipment item	Column section	Beam section	Brace section	Height	Young′s modulus
Surge arrester	C400×10	----	----	2.85 m	2×10^{5} MPa
Current transformer	L80×80×8	L100×100×10	L50×50×5	3.14 m	2×10^{5} MPa

Table 5 Second-moment parameters of random variables with lognormal distribution

Random variable	Mean	Standard deviation	COV(%)	Distribution
Steel yield strength (Pa)	2.35×10^{8}	2.35×10^{7}	10.0	LN(9.27,0.01)
Porcelain elasticity modulus (Pa)	9.40×10^{10}	1.29×10^{10}	13.7	LN(25.26,0.137)
Porcelain ultimate strength (Pa)	5.05×10^{7}	1.03×10^{7}	20.3	LN(17.72,0.20)
Porcelain density (kg/m^3)	2415.55	189.06	7.8	LN(7.79,0.08)
Mass at top of surge arrester (kg)	258.00	25.80	10.0	LN(5.55,0.01)
Mass at top of current transformer (kg)	953.92	95.39	10.0	LN(6.86,0.01)

to the leak of oil and loss of electrical functionality. The response thresholds corresponding to moderate and extensive damage states are considered as 25% and 50% of porcelain ultimate strength, per the recommendation of IEEE 693 (2005). These thresholds also were suggested in previous studies, such as (Baghmisheh and Estekanchi, 2019; Mohammadpour, 2017; Zareei *et al*., 2017), in which the seismic fragility of equipment was examined. Note that since fragility curves result in an intensity measure or a structural response and produce the probability of exceedance, they cannot directly be used. However, fragility models can be employed to estimate the damage ratio corresponding to each intensity measure or structural response. Since the damage ratio is a physical quantity, it can be utilized in this procedure. A more detailed explanation of using fragility models in reliability analysis is provided in Mahsuli and Haukaas (2013a). To quantify the monetary loss associated with each damage state, a simple repair cost model is developed. It is assumed that a stress response lower than the moderate damage state threshold causes no economic loss. On the other hand, when the stress response exceeds the extensive damage state threshold, the equipment needs to be replaced, which means repair cost is equal to the replacement cost of the damaged equipment. The stress value falls between these two thresholds. The damage ratio, that is, the ratio of repair cost to replacement cost, is expressed by a sine function as follows:

$$\eta = 0.7\sin(\pi\cdot(\frac{\sigma_{\max j}}{0.5\sigma_{\mathrm{u}}}-0.5))+0.3 \tag{8}$$

where η_j is the damage ratio for equipment j; σ_{u} is the ultimate strength of porcelain; and $\sigma_{\max,j}$ is the maximum stress response at the bottom section of the porcelain column. The bottom section of the columns, where the induced flexural moment reaches maximum, has been recognized in past studies as a critical section of the porcelain columns (see Alessandri *et al*., 2015; Zareei *et al*., 2017)). Hence, the maximum stress response at the bottom of the porcelain column is utilized in the repair cost model. By computing the damage ratio, the repair cost can be obtained through the following simple expression:

$$l_j = \eta\cdot C_{\mathrm{e}j}\cdot\varepsilon_{\mathrm{c}j} \tag{9}$$

Table 6 Second-moment parameters of random variables with uniform distribution

	Insulators′ outer diameter (m)	
Porcelain unit	Lower bound	Upper bound
Surge arrester	0.320	0.420
Current transformer	0.430	0.530

in which, l_j, is the repair cost of equipment j, $C_{\mathrm{e}j}$ is the replacement cost of the equipment j, and $\varepsilon_{\mathrm{c}j}$ is the error aspect of the repair cost model. The error is modeled by a random variable with normal distribution whose mean and standard deviation are zero and 0.1, respectively. According to the equipment catalog, the replacement cost of SA and CT are \$1.0 and \$3.3 thousand. By assuming that there are nine items of each type of equipment in the considered high-voltage substation, the total value of the equipment in the substation is equal to \$38.7 thousand. Note that the considered repair cost model is a simple one to demonstrate the algorithm proposed for performing detailed risk analysis on substation equipment. To obtain more realistic results, a more complicated repair cost model should be developed in the future which would preferably be calibrated with data taken from previous earthquakes.

As explained in Section 2, scenario sampling requires the accumulation of cost over a period of time, for instance, 50 years. Since the value of the loss at different times varies, the discounting model is employed to transfer the future value of loss to the current value. Thus, this model depends on the time of earthquake occurrence in the simulated sample. The expression of this model appears below:

$$l_{\mathrm{p}} = l_{\mathrm{f}}\cdot\exp(-r\cdot t) \tag{10}$$

where l_{p} and l_{f} are the current and future value of the loss, r is the rate of effective annual profit, and t is the time parameter. In this study, the rate of effective annual profit is modeled by a normally distributed random variable with a mean of 3% and a coefficient of variation of 10%.

It is noteworthy that the proposed procedure is not limited to this simple repair cost model. Other complicated models are applicable in the proposed procedure as long as they satisfy probabilistic models′ regulations, as described in Section 3. Note that the

proposed detailed seismic risk analysis framework makes possible consideration of various seismic losses associated with equipment damage and power outages, such as losses due to the interruption of business or an emergency response. These undirected losses are applicable in the comprehensive risk analysis of a whole substation. Since a single system of equipment is examined in the case study of the proposed framework, only the direct loss of equipment is taken into account.

4 Application

This section investigates the application of the proposed detailed reliability-based risk analysis to estimate substation equipment losses. The risk analyses considered under various earthquake scenarios are conducted in accordance with the proposed procedure described in Section 2 to compute the loss associated with each scenario. Models introduced in Section 3 are employed to perform risk analysis. The results of analyses are presented in the form of the exceedance probability of loss. Subsequently, various risk measures are defined to summarize and compare loss results.

4.1 Earthquake scenarios

Computing accumulated loss in the life cycle of the structures, which is a common scenario found in risk assessment studies, is considered here. Furthermore, occurrences of earthquakes with a specific magnitude or return period are also utilized as earthquake scenarios to demonstrate the applicability of the procedure. The reason for selecting these scenarios is that they are sometimes more convenient in terms of communicating risk to non-engineering decisionmakers. For instance, the expected losses resulting from an earthquake with a magnitude of seven is more comprehensible for non-technical persons. The following sections introduce scenarios and present their risk analysis results.

4.1.1 Scenarios with a specific magnitude

Three scenarios with a specific magnitude, including M=5, 6, and 7, entitled hereafter Scenario 1, 2, and 3, respectively, are considered herein. Recall that performing risk analysis for scenarios with a specific magnitude requires substituting the magnitude model in the chain of probabilistic models with a constant value. That is, for each sample of a simulation, an earthquake with a specific magnitude occurs in one of the seismic sources. Responses of subsequent models are then calculated, which finally results in a loss curve. As a byproduct of the procedure, the probability distribution of engineering demand parameters can also be obtained. Figure 7 depicts the complementary cumulative distribution function of key structural responses, i.e., the maximum relative displacement between equipment and the maximum stress on porcelain, along with the coefficient of variation of the calculated probabilities resulting from 20000 samples under the scenario M=7. As previously observed, the distribution of maximum stresses for CT is slightly larger than that for SA.

Figure 8 illustrates the EP of loss, i.e., the loss curve, for earthquake scenarios with magnitudes 5, 6, and 7. The vertical axis of this figure is presented in the logarithmic scale to better show the tail of the distribution. The loss values in the horizontal axis are normalized to the total value of the equipment in the substation, i.e., \$38.7 thousand. These curves are produced for each individual piece of equipment and its system. As expected, the larger the magnitude of the scenario, the greater the loss. The distance between loss curves of various magnitudes is high at lower loss values. However, by proceeding along the x-axis toward larger loss values, this difference diminishes.

The results of risk analysis for each scenario are obtained by simulating 20,000 samples. According to Eq. (5), the minimum required samples are 19,600 samples in order to estimate the probability of exceedance greater than 0.02, with the coefficient of variation below 5%. To provide a sense of the accuracy of these results, the loss curve of the SA-CT system shown in Fig. 8(c) under scenario 3, i.e., an earthquake with magnitude 7, is scrutinized. The probability of exceeding \$3 thousand under this scenario is 12.2%, while the probability of exceeding \$4.5 thousand is 2.6%. The coefficients of variation of the computed probabilities are 1.9% and

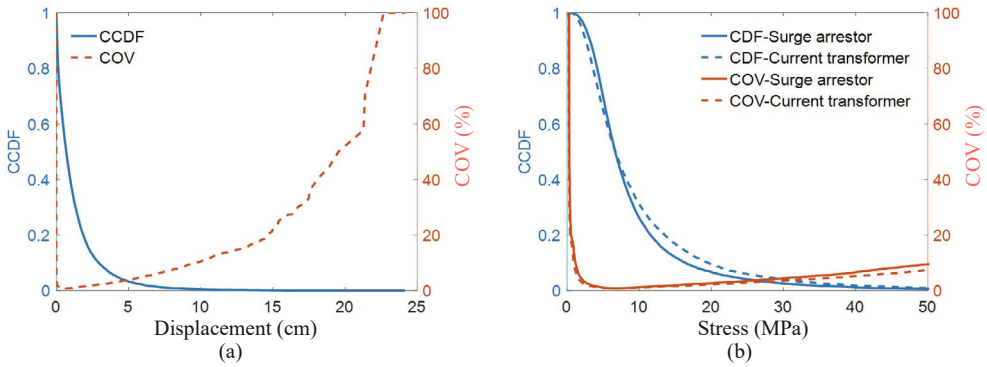

Fig. 7 Complementary cumulative distribution function of maximum: (a) tip relative displacement response between equipment, and (b) the stress response at the bottom of porcelain

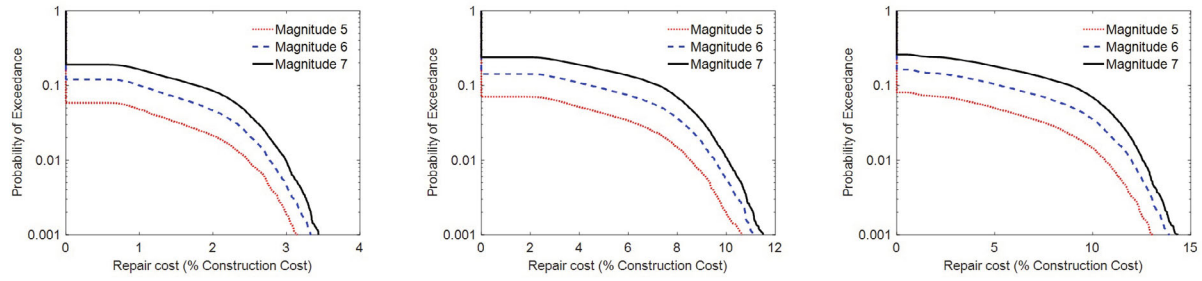

Fig. 8 Loss curves of scenarios with specific moment magnitude for (a) surge arrester, (b) current transformer, and (c) SA-CT system

4.3%, respectively. This reveals the accuracy of the computed probabilities.

4.1.2 Scenarios with a specific return period

Three scenarios with a specific return period, including RP=72, 475, and 2,475 years, hereafter referred to as scenarios 4, 5, and 6, are considered. Performing risk analysis for these scenarios requires specification of earthquake intensity corresponding to each return period. To this end, the hazard curve proposed by Gholipour *et al*. (2008) for a site in Tehran is employed. Figure 9 shows this curve along with PGA values corresponding to 72, 475, and 2,475 years as return periods. To perform risk analysis for a scenario with a specific return period, the maximum acceleration of artificial ground motions is scaled to the PGA value obtained from the hazard curve. Figure 10 compares the resulting loss curves for the three return periods. Similar to Fig. 8, loss values are normalized to the total value of SAs and CTs in the substation. The loss curves of the scenario with 2,475 years RP are, as expected, above those of the other scenarios. As seen, there is a considerable difference between loss curves of 72 years RP and those of the other scenarios, whereas this difference is slight between 475 and 2,475 years RP. This can be attributed to the fact that earthquakes with 475 years RP induce severe damage, which yields nearly similar loss curves for 475 and 2,475 years RP.

4.1.3 Total loss in the life cycle

The total loss in the life cycle of structures, i.e., 50 years, is considered as Scenario 7. Figure 11 illustrates the exceedance probability of the accumulated loss in a 50-year period, normalized to the total value of equipment in the substation, i.e., \$38.7 thousand. To preform risk analysis under this scenario, all of the probabilistic models displayed in Fig. 2 are employed. Risk analysis is conducted using scenario sampling, as explained in Section 2. Note that each seismic source contributes to the resulting loss curve in accordance with its occurrence rate in this scenario. As expected, it is observed that the total loss of the SA-CT system is greater than those of individual equipment. This figure reveals that the current transformer makes a larger contribution to the total loss than does the surge arrester. Thus, high prioritization should be allocated to retrofit the CT in the considered system. This is one of the crucial insights that can be obtained using the proposed approach.

4.2 Risk measures

To make risk-based design and retrofit decisions, using the whole loss curve may not be practical. Thus,

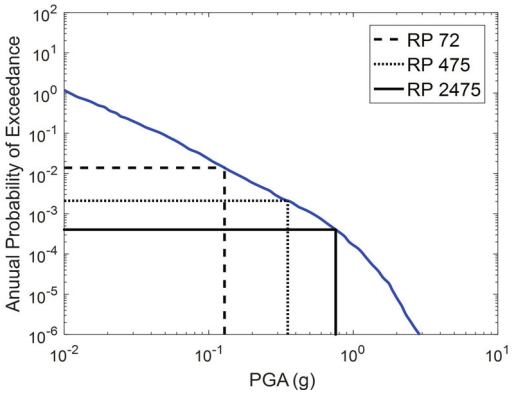

Fig. 9 The hazard curve for a site in Tehran

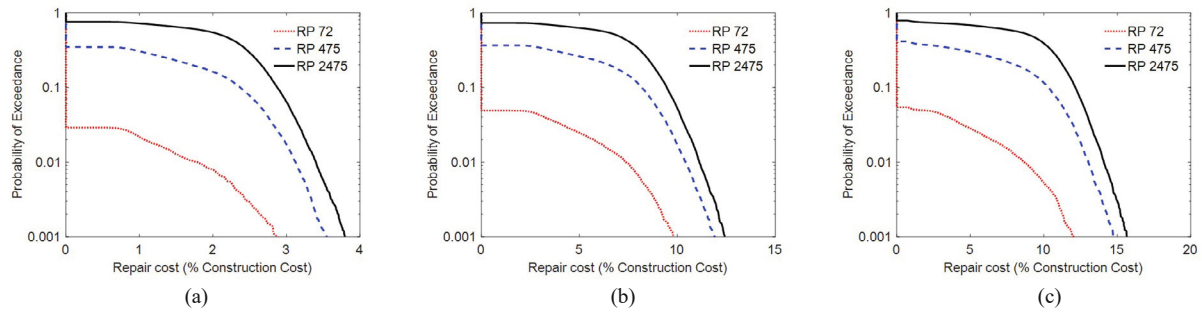

Fig. 10 Loss curves of scenarios with specific return periods for (a) a surge arrester, (b) a current transformer, and (c) a SA-CT system

a risk measure should be extracted from the loss curve. For this purpose, several risk measures are discussed herein. According to the attitude of the stakeholder, i.e., risk-neutral or risk-averse, one of these measures may be utilized to render a risk-based decision.

The expected cost is a common risk measure that stakeholders have employed to reach a design decision. By considering c as the realization of the random variable representing cost, the $f_C(c)$ denotes the probability distribution function of cost, and $G_C(c)$ denotes the complementary cumulative distribution function, i.e., the loss curve. The area under the curve is the expected cost, calculated using the following integral:

$$\mu_c = \int_0^\infty c \cdot f_C(c)\mathrm{d}c = -\int_0^\infty c \cdot \frac{\mathrm{d}G_C(c)}{\mathrm{d}c}\mathrm{d}c = \int_0^\infty G_C(c)\mathrm{d}c \tag{11}$$

The probability that cost exceeds a specific threshold, c_o, can be treated as another risk measure. This probability can be calculated by limit state function $g=c-c_o$, or it can be extracted from the loss curve, i.e., $p_c=G(c_o)$. Selecting a specific value for c_o implies that the decisionmaker is concerned with the exceedance probability of that amount of loss. The level of risk aversion for this measure depends on the value selected for c_o. The reverse of the above-mentioned risk measure, i.e., the cost value at a selected exceedance probability, p_o, is another considered risk measure. This measure can be calculated by the inverse function of the EP curve, $q_c=G^{-1}(p_o)$. The q_c hereafter is called the value-at-risk. A reasonable choice for p_o is 1%, which is the suggested risk level for 50 years in ASCE 7/SEI 16 (2017). These measures differ in their effectiveness in communicating risk. The expected cost, μ_c, and the exceedance probability of cost p_c, are more understandable measures for non-engineering decisionmakers than the value-at-risk q_c. Thus, the expected cost and the exceedance probability of cost may be used to communicate risk for risk-neutral and risk-averse clients, respectively. On the contrary, the value-at-risk may be used to communicate risk to a technical audience.

The introduced risk measures are calculated and represented in Fig. 12 for three scenarios, including the occurrence of an earthquake with M=7 (Scenario 3), the occurrence of an earthquake with RP=2,475 years

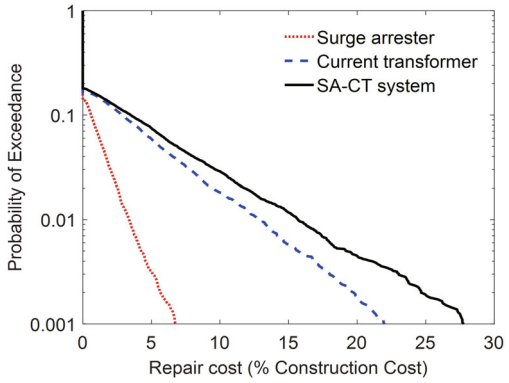

Fig. 11 Accumulated loss curves of equipment for a 50-year period

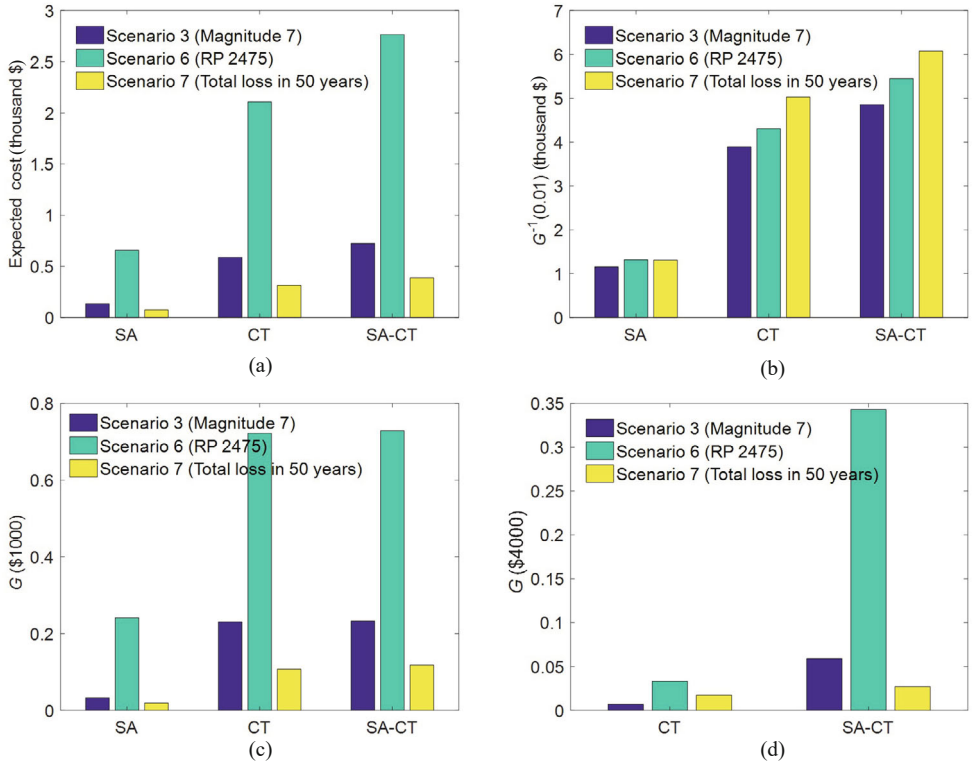

Fig. 12 Comparing the risk of three scenarios in terms of (a) expected cost, (b) the cost at a 1% probability of exceedance, (c) an exceedance probability of $1000, and (d) an exceedance probability of $4000 as the risk measure

(Scenario 6), and the occurrence of an earthquake in accordance with the rate of each seismic source over a 50-year period (Scenario 7). The higher the bar in this figure, the higher the risk associated with that scenario or equipment. As seen in terms of all risk measures, the CT equipment has a higher risk factor and priority for the retrofit than does the SA. In three of four risk measures, the risk associated with Scenario 6 is the greatest, and Scenario 7 the least. This is mainly because a major earthquake with 2,475 RP, which corresponds to large loss values, occurs in each sample of risk analysis under Scenario 6. However, the earthquake occurs in accordance with the rate of seismic source and magnitude model under Scenario 7, which may be a low- or moderate-level earthquake.

5 Conclusions

This paper proposes a reliability-based risk analysis procedure to evaluate the seismic loss of substation equipment by considering substantial uncertainties. In contrast to previous risk analysis approaches for substation equipment that calculate the expected cost by summing construction costs and the product of failure probability to repair costs, this study considers total cost as a random variable whose probability distribution depends upon many probabilistic models and random variables. This makes it possible to explicitly consider uncertainties involved in the calculation of loss. Despite existing risk assessment approaches for infrastructure components at the regional level that provide a rough estimate of loss, this approach employs more refined models, thereby increasing the precision of loss estimation. This procedure takes into account uncertainties involved in hazard, response, and loss by utilizing random variables and probabilistic models. Reliability analysis is conducted on the chain of probabilistic models to evaluate the limit state function that is defined regarding loss. The analysis results in the exceedance probability of loss, i.e., a loss curve.

The application of the proposed framework is demonstrated in the loss estimation of interconnected electrical equipment located at a substation in Tehran under the effects of several earthquake scenarios. To this end, the deterministic finite element model of equipment is developed and verified. This model is treated as a probabilistic finite element model by considering random variables for uncertainties associated with the material, mass, and geometric properties of the equipment. Next, models for the occurrence, location, magnitude, and intensity of an earthquake are adopted from the literature and used herein. These models, in conjunction with a proposed simple repair cost model, construct a chain of the probabilistic models that are subjected to the Monte Carlo sampling analysis to estimate the EP of loss. The accuracy of the procedure is demonstrated by using the coefficient of variations of the computed probabilities, which is less than 4.5% for large loss values. Furthermore, four risk measures extracted from the loss curve are discussed. These measures, which summarize results of risk analysis, can be utilized by decisionmakers to prioritize equipment for rehabilitation or to optimize their designs. In the case study here, it is found that the current transformer imposes more total loss than the surge arrester in terms of all risk measures, thus creating a higher priority for a retrofit. Note that the proposed framework is not limited to power infrastructure components and it can be employed to quantify the risk for other infrastructure components.

References

Aghababaei M and Mahsuli M (2018), "Detailed Seismic Risk Analysis of Buildings Using Structural Reliability Methods," *Probabilistic Engineering Mechanics*, **53**(April 2017): 23–38. https://doi.org/10.1016/j.probengmech.2018.04.001

Alessandri S, Giannini R, Paolacci F, Amoretti M and Freddo A (2015), "Seismic Retrofitting of an HV Circuit Breaker Using Base Isolation with Wire Ropes, Part 2 : Shaking-Table Test Validation," *Engineering Structures*, **98**: 263–274. https://doi.org/10.1016/j.engstruct.2015.03.031

Alessandri S, Giannini R, Paolacci F and Malena M (2015), "Seismic Retrofitting of an HV Circuit Breaker Using Base Isolation with Wire Ropes, Part 1: Preliminary Tests and Analyses," *Engineering Structures*, **98**: 251–262.

Altieri D, Tubaldi E, De Angelis M, Patelli E and Dall′Asta A (2018), "Reliability-Based Optimal Design of Nonlinear Viscous Dampers for the Seismic Protection of Structural Systems," *Bulletin of Earthquake Engineering*, **16**(2): 963–982.

Ansal A, Akinc A, Cultrera G, Erdik M, Pessina V, Tönük G and Ameri G (2009), "Loss Estimation in Istanbul Based on Deterministic Earthquake Scenarios of the Marmara Sea Region (Turkey)," *Soil Dynamics and Earthquake Engineering*, **29**(4): 699–709.

Apostolakis G, Qu B, Ecemis N and Dogruel S (2007), "Field Reconnaissance of the 2007 Niigata-Chuetsu Oki Earthquake," *Earthquake Engineering and Engineering Vibration*, **6**(4): 317–330.

ASCE-7 (2017), *Minimum Design Loads and Associated Criteria for Buildings and Other Structures*, USA. https://doi.org/10.1061/9780784414248

ATC-1 (1985), *Earthquake Damage Evaluation for California, Redwood City, California*, Applied Technology Council, USA.

Azevedo J, Guerreiro L, Bento R, Lopes M and Proença J (2010), "Seismic Vulnerability of Lifelines in the Greater Lisbon Area," *Bulletin of Earthquake Engineering*, **8**(1): 157–180.

Bagen B, Huang D and Fattal K (2019), "Enhanced Probabilistic Approach for Substation Reliability

Assessment," *IET Generation, Transmission & Distribution*, **13**(12): 2488–2495.

Baghmisheh AG and Estekanchi HE (2019), "Effects of Rigid Bus Conductors on Seismic Fragility of Electrical Substation Equipment," *Soil Dynamics and Earthquake Engineering*, **125**: 105733.

Baghmisheh AG and Estekanchi HE (2021), "Quantifying Seismic Response Uncertainty of Electrical Substation Structures Using Endurance Time Method," *Structures*, **30**: 838–849.

Baghmisheh AG and Mahsuli M (2021), "Seismic Performance and Fragility Analysis of Power Distribution Concrete Poles," *Soil Dynamics and Earthquake Engineering*, **150**: 106909.

Baghmisheh GA and Estekanchi HE (2020), "Influence of Dynamic Interaction Between Interconnected Electrical Substation Equipment on Seismic Response," *Journal of Structural and Construction Engineering*. https://doi.org/10.22065/jsce.2020.171843.1784

Bai W, Dai J, Zhou H, Yang Y and Ning X (2017), "Experimental and Analytical Studies on Multiple Tuned Mass Dampers for Seismic Protection of Porcelain Electrical Equipment," *Earthquake Engineering and Engineering Vibration*, **16**(4): 803–813.

Bai W, Moustafa MA and Dai JW (2019), "Seismic Fragilities of High-Voltage Substation Disconnect Switches," *Earthquake Spectra*, **35**(4): 1559–1582.

Bayari MA, Shabakhty N and Abadi EIZ (2022), "Analyzing Uncertainties Involved in Estimating Collapse Risk with and Without Considering Uncertainty Probability Distribution Parameters," *Earthquake Engineering and Engineering Vibration*, **21**(1): 101–116.

Castaldo P and Amendola G (2021), "Optimal DCFP Bearing Properties and Seismic Performance Assessment in Nondimensional Form for Isolated Bridges," *Earthquake Engineering and Structural Dynamics*, **50**(9): 2442–2461.

Castaldo P, Amendola G and Palazzo B (2017a), "Seismic Fragility and Reliability of Structures Isolated by Friction Pendulum Devices: Seismic Reliability-Based Design (SRBD)," *Earthquake Engineering and Structural Dynamics*, **46**(3): 425–446.

Castaldo P, Mancini G and Palazzo B (2018a), "Seismic Reliability-Based Robustness Assessment of Three-Dimensional Reinforced Concrete Systems Equipped with Single-Concave Sliding Devices," *Engineering Structures*, **163**: 373–387.

Castaldo P, Palazzo B, Alfano G and Palumbo MF (2018b), "Seismic Reliability-Based Ductility Demand for Hardening and Softening Structures Isolated by Friction Pendulum Bearings," *Structural Control and Health Monitoring*, **25**(11): e2256.

Castaldo P, Palazzo B and della Vecchia P (2016), "Life-Cycle Cost and Seismic Reliability Analysis of 3D Systems Equipped with FPS for Different Isolation Degrees," *Engineering Structures*, **125**: 349–363.

Castaldo P, Palazzo B and Ferrentino T (2017b), "Seismic Reliability-Based Ductility Demand Evaluation for Inelastic Base-Isolated Structures with Friction Pendulum Devices," *Earthquake Engineering & Structural Dynamics*, **46**(8): 1245–1266.

Cornell CA and Krawinkler H (2000), "Progress and Challenges in Seismic Performance Assessment," *PEER Center News 3*, University of California, Berkeley, USA.

D′Ayala D and Ansal A (2012), "Non-Linear Push Over Assessment of Heritage Buildings in Istanbul to Define Seismic Risk," *Bulletin of Earthquake Engineering*, **10**(1): 285–306.

Der Kiureghian A and Ang AHS (1977), "A Fault-Rupture Model for Seismic Risk Analysis," *Bulletin of the Seismological Society of America*, **67**(4): 1173–1194.

Der Kiureghian A and Zhang Y (1999), "Space-Variant Finite Element Reliability Analysis," *Computer Methods in Applied Mechanics and Engineering*, **168**(1–4): 173–183.

FEMA (2003), *Multi-Hazard Loss Estimation Methodology: Earthquake Model*, Department of Homeland Security, Washington, DC, USA.

FEMA 58-1 (2012), *Seismic Performance Assessment of Buildings* (*Volume 1-Methodology*), Federal Emergency Management Agency, Washington, USA.

Filiatrault AKS (2000), "Seismic Interaction of Interconnected Electrical Substation Equipment," *Journal of Structural Engineering*, **126**(10): 1140–1149. https://doi.org/10.1016/S0950-1401(10)04009-7

Gholipour Y, Bozorgnia Y, Rahnama M and Berberian MSJ (2008), "Probabilistic Seismic Hazard Analysis, Phase I-Greater Tehran Regions," *Final Report*, Iran.

Gino D, Castaldo P, Giordano L and Mancini G (2021), "Model Uncertainty in Non-Linear Numerical Analyses of Slender Reinforced Concrete Members," *Structural Concrete*, **22**(2): 845–870. https://doi.org/10.1002/suco.202000600

Gökçe T, Yüksel E and Orakdöğen E (2019), "Seismic Performance Enhancement of High-Voltage Post Insulators by a Polyurethane Spring Isolation Device," *Bulletin of Earthquake Engineering*, **17**(3): 1739–1762.

Haukaas T (2008), "Unified Reliability and Design Optimization for Earthquake Engineering," *Probabilistic Engineering Mechanics*, **23**(4): 471–481.

He J and Li J (2004), "Seismic Reliability Analysis of Large Electric Power Systems," *Earthquake Engineering and Engineering Vibration*, **3**(1): 51–55.

IEEE Standard 693 (2005), *IEEE Recommended Practice for Seismic Design of Substations*, Revision of IEEE 693-1985 & 1997, USA.

Jahangiri V and Shakib H (2020), "Reliability-Based Seismic Evaluation of Buried Pipelines Subjected to Earthquake-Induced Transient Ground Motions,"

Bulletin of Earthquake Engineering, **18**(8): 3603–3627.

Jaigirdar MA (2005), "Seismic Fragility and Risk Analysis of Electric Power Substations," *PhD Thesis*, McGill University, Canada.

Khalvati AH and Hosseini M (2009), "Seismic Performance of Electrical Substations' Equipments in Bam Earthquake (Iran 2003)," In *TCLEE 2009: Lifeline Earthquake Engineering in a Multihazard Environment*, pp. 1–8.

Kitayama S and Constantinou MC (2019), "Probabilistic Seismic Performance Assessment of Seismically Isolated Buildings Designed by the Procedures of ASCE/SEI 7 and Other Enhanced Criteria," *Engineering Structures*, **179**: 566–582.

Kongar I, Esposito S and Giovinazzi S (2017), "Post-Earthquake Assessment and Management for Infrastructure Systems: Learning from the Canterbury (New Zealand) and L′Aquila (Italy) Earthquakes," *Bulletin of Earthquake Engineering*, **15**(2): 589–620.

Kulhawy FH, Phoon KK, Prakoso WA and Hirany A (2007), "Reliability-Based Design of Foundations for Transmission Line Structures," In *Electrical Transmission Line and Substation Structures: Structural Reliability in a Changing World*, pp. 184–194.

Kwasinski A, Eidinger J, Tang A and Tudo-Bornarel C (2014), "Performance of Electric Power Systems in the 2010–2011 Christchurch, New Zealand, Earthquake Sequence," *Earthquake Spectra*, **30**(1): 205–230.

Li J, Wang T and Shang Q (2019), "Probability-Based Seismic Reliability Assessment Method for Substation Systems," *Earthquake Engineering and Structural Dynamics*, **48**(3): 328–346.

Li S, Tsang HH, Cheng Y and Lu Z (2017), "Effects of Sheds and Cemented Joints on Seismic Modelling of Cylindrical Porcelain Electrical Equipment in Substations," *Earthquakes and Structures*, **12**(1): 55–65.

Mahsuli M and Haukaas T (2012), "Computer Program for Multimodel Reliability and Optimization Analysis," *Journal of Computing in Civil Engineering*, **27**(1): 87–98.

Mahsuli M and Haukaas T (2013a), "Seismic Risk Analysis with Reliability Methods, part I : Models," *Structural Safety*, **42**: 54–62. https://doi.org/10.1016/j.strusafe.2013.01.003

Mahsuli M and Haukaas T (2013b), "Seismic Risk Analysis with Reliability Methods, part II: Methods," *Structural Safety*, **42**: 63–74.

Mahsuli, M, Rahimi H and Bakhshi A (2018), "Probabilistic Seismic Hazard Analysis of Iran Using Reliability Methods," *Bulletin of Earthquake Engineering*, **17**: 1117–1143.

McGuire RK (2004), *Seismic Hazard and Risk Analysis*, Earthquake Engineering Research Institute, Oakland, USA.

McKenna F, Fenves G and Filippou FC MS (2000), *Open System for Earthquake Engineering Simulation* (*OpenSees*), *PEERC*, USA.

Moehle J and Deierlein GG (2004), "A Framework Methodology for Performance-Based Earthquake Engineering," In *13th World Conference on Earthquake Engineering*, *Paper No. 679*, Vancouver, Canada.

Mohammadi RK, Nikfar F and Akrami V (2012), "Estimation of Required Slack for Conductors Connecting Substation Equipment Subjected to Earthquake," *IEEE Transactions on Power Delivery*, **27**(2): 709–717.

Mohammadi RK and Tehrani AP (2014), "An Investigation on Seismic Behavior of Three Interconnected Pieces of Substation Equipment," *IEEE Transactions on Power Delivery*, **29**(4): 1613–1620.

Mohammadpour SHM (2017), "Experimental System Identification of a 63kV Substation Post Insulator and Developing Its Fragility Curves by Dynamic Fnite Element Analyses," *Earthquake Spectra*, **33**(3): 1149–1172.

Mohsenian V, Hajirasouliha I and Filizadeh R (2021), "Seismic Reliability Analysis of Steel Moment-Resisting Frames Retrofitted by Vertical Link Elements Using Combined Series–Parallel System Approach," *Bulletin of Earthquake Engineering*, **19**(2): 831–862.

Narjabadifam P, Hoseinpour R, Noori M and Altabey W (2021), "Practical Seismic Resilience Evaluation and Crisis Management Planning Through GIS-Based Vulnerability Assessment of Buildings," *Earthquake Engineering and Engineering Vibration*, **20**(1): 25–37.

Palanci M (2019), "Fuzzy Rule Based Seismic Risk Assessment of One-Story Precast Industrial Buildings," *Earthquake Engineering and Engineering Vibration*, **18**(3): 631–648.

Paolacci F, Giannini R, Alessandri S and De Felice G (2014), "Seismic Vulnerability Assessment of a High Voltage Disconnect Switch," *Soil Dynamics and Earthquake Engineering*, **67**: 198–207. https://doi.org/10.1016/j.soildyn.2014.09.014

Papagiannopoulos GA, Hatzigeorgiou GD and Beskos DE (2012), "An Assessment of Seismic Hazard and Risk in the Islands of Cephalonia and Ithaca, Greece," *Soil Dynamics and Earthquake Engineering*, **32**(1): 15–25.

Rezaeian S and Der Kiureghian A (2012), "Simulation of Orthogonal Horizontal Ground Motion Components for Specified Earthquake and Site Characteristics," *Earthquake Engineering & Structural Dynamics*, **41**(2): 335–353.

Shang Q, Guo X, Li Q, Xu Z, Xie L, Liu C, *et al*. (2020), "A Benchmark City for Seismic Resilience Assessment," *Earthquake Engineering and Engineering Vibration*, **19**(4): 811–826.

Sudret B and Der Kiureghian A (2002), "Comparison of Finite Element Reliability Methods," *Probabilistic Engineering Mechanics*, **17**(4): 337–348.

Takada S, Bastami M, Kuwata Y and Javanbarg MB

(2004), "Performance of Electric Power Systems During the Bam Earthquake and Its Fragility Analyses," *Memoirs of Construction Engineering Research Institute*, **46**: 152–161.

Takhirov S, Fenves G and Fujisaki E (2004), "Seismic Qualification and Fragility Testing of Line Break 550-kV Disconnect Switches," *Report 2004/08*, Pacific Earthquake Engineering Research Center (PEER), University of California, Berkeley, USA.

Yang SC, Liu TJ and Hong HP (2017), "Reliability of Tower and Tower-Line Systems Under Spatiotemporally Varying Wind or Earthquake Loads," **143**(10): 1–13. https://doi.org/10.1061/(ASCE)ST.1943-541X.0001835

Yang TY, Moehle J, Stojadinovic B and Der Kiureghian A (2009), "Seismic Performance Evaluation of Facilities: Methodology and Implementation," *Journal of Structural Engineering*, **135**(10): 1146–1154.

Yang Z, Xie Q, He C and Xue S (2021), "Numerical Investigation of the Seismic Response of a UHV Composite Bypass Switch Retrofitted with Wire Rope Isolators," *Earthquake Engineering and Engineering Vibration*, **20**(1): 275–290.

Zareei SA, Hosseini M and Ghafory-Ashtiany M (2017), "Evaluation of Power Substation Equipment Seismic Vulnerability by Multivariate Fragility Analysis: A Case Study on a 420 kV Circuit Breaker," *Soil Dynamics and Earthquake Engineering*, **92**: 79–94. https://doi.org/10.1016/j.soildyn.2016.09.026

Zheng HD, Fan J and Long XH (2017), "Analysis of the Seismic Collapse of a High-Rise Power Transmission Tower Structure," *Journal of Constructional Steel Research*, **134**: 180–193.

Zheng X and Li H (2022), "Life-Cycle Failure Probability Analysis of Deteriorated RC Bridges Under Multiple Hazards of Earthquakes and Strong Winds," *Earthquake Engineering and Engineering Vibration*, **21**(3): 811–823.